

Prediction of scour around single vertical piers with different cross-section shapes

Amir Bordbar^{*}, Soroosh Sharifi and Hassan Hemida

School of Engineering, University of Birmingham, Birmingham, UK

(Received May 23, 2020, Revised February 24, 2021, Accepted February 26, 2021)

Abstract. In the present work, a 3D numerical model is proposed to study local scouring around single vertical piers with different cross-section shapes under steady-current flow. The model solves the flow field and sediment transport processes using a coupled approach. The flow field is obtained by solving the Unsteady Reynolds Averaged Navier-Stokes (URANS) equations in combination with the $k-\omega$ SST turbulence closure model and the sediment transport is considered using both bedload and suspended load models. The proposed model is validated against the empirical measurements of local scour around single vertical piers with circular, square, and diamond cross-section shapes obtained from the literature. The measurement of scour depth in equilibrium condition for the simulations reveal the differences of 4.6%, 6.7% and 13.1% from the experimental measurements for the circular, square, and diamond pier cases, respectively. The model displayed a remarkable performance in the prediction of scour around circular and square piers where horseshoe vortices (HSVs) have a leading impact on scour progression. On the other hand, the maximum deviation was found in the case of the diamond pier where HSVs are weak and have minimum impact on the formation of local scour. Overall, the results confirm that the prediction capability of the present model is almost independent of the strength of the formed HSVs and pier cross-section shapes.

Keywords: scour; steady current flow; sediment transport; bridge piers; offshore wind turbine

1. Introduction

The existence of a marine structure under a flow field substantially changes the behavior of the flow, creating a complex 3D flow behavior with separation, swirling, and recirculation motions. For marine structures mounted on an erodible seabed or riverbed (i.e., sandy bed) these changes can be strong enough to wash out part of the sediments adjacent to the structure, a process known as scouring, which is of importance in connection with the stability of the structure (Sumer *et al.* 1993). In the case of bridge piers, scouring around piers is the most frequent cause of bridge failure which causes significant maintenance and repair costs (Topczewski *et al.* 2016). Similarly, in the offshore wind industry, scouring around the piles of shallow water wind turbines have a significant effect on the stability of this structure. Observations show that the maximum possible scour around a pile in an unprotected bed can be up to twice the size of the pile diameter (Sumer and Fredsøe 2001a). This means that typical piles foundation length have to be overdesigned for an extra 8-10 m, which imposes a huge extra cost (Hansen *et al.* 2007). Hence, protecting piles/piers from scour damage in

^{*}Corresponding author, Ph.D. Candidate, E-mail: Abordbar182@gmail.com

an economically efficient way is a considerable engineering challenge, which can be achieved by safe design of the pile's foundation against scour damage or applying scour protection systems such as installing a scour protection mattress or rock armor.

To better understand scouring and the factors affecting it, extensive experimental investigations have been carried out over the past few decades. A large number of these studies focus on turbulence structures on rigid flat beds and investigate the formation of horseshoe vortices (HSVs), due to adverse pressure gradient, and lee-wake vortices as primitive mechanisms of scouring upstream and downstream of pile/piers, respectively. Works of Baker (1980), Dargahi (1989), Seal and Smith (1999) and Agui and Andreopoulos (1992) are noticeable studies in this group. Additionally, various experimental investigations of scouring on mobile beds have been conducted in both river and marine environments. For instance, Dargahi (1990) and Melville and Chiew (1999) experimentally investigated the formation of scouring around a circular cylinder in steady current, and attempted to explain the evolution of scouring from the early to final stages. Sumer *et al.* (1992) and Sumer *et al.* (1993) did a series of experiments for investigating scouring around circular, square and diamond cross-section columns for both steady and wave-current flows. Dey *et al.* (1995) and Graf and Istiarto (2002) carried out a wide range of tests for measuring flow patterns around circular cylinders mounted in a scour hole.

Numerical modelling has also been widely used by several researchers to understand flow and scour mechanisms. Tseng *et al.* (2000), Salaheldin *et al.* (2004), Kirkil *et al.* (2005), Kirkil *et al.* (2008) and Kirkil *et al.* (2009), and loads of others studied the flow behavior around pile/piers on rigid bed. In these works, different hydrodynamic models were employed to better understand the formation of horseshoe and wake vortex structures and the bed shear stress distribution on both rigid flat and scoured beds around piles. On the other hand, a massive number of studies attempted to model local scouring process around piles/piers. A group of them carried out the modelling by coupling a hydrodynamic model with a morphodynamic model to simulate the time development of scour evolution, which is specified as a classical approach here. In classical approach, a boundary (e.g., bottom or bed) of the numerical domain is presented as a sandy bed-water interface, and deformation of this boundary due to scour is provided by solving a mass conservation equation on the boundary as a result of sediment transport. An early example of this approach for modelling of scour around the piles/piers dates back to the nineties when Olsen and Melaaen (1993) and Olsen and Kjellesvig (1998) developed the first 3D model for predicting local scour on a mobile bed for clear water regime and cohesionless sediment conditions. However, their model lacked the transient term, and thus, was unable to predict the maximum scour depth correctly. In a notable work, Roulund *et al.* (2005) investigated the flow and scour around a vertical pile both numerically and experimentally in a live-bed with non-cohesive sand. They also developed a 2D numerical description model for the bedload which was an extension of the bedload model in Engelund and Fredsøe (1976). However, their scour simulation model did not incorporate suspended sediment transport, and the flow model used a steady solution. Therefore, it was incapable of predicting the formation of lee-wake vortices behind the pile. Göthel and Zielke (2007) presented a model for predicting scour around a cylinder pile exposed to steady and wave currents. However, similar to Roulund *et al.* (2005) approach, their model only included bedload transport and ignored the suspended load. They numerically modelled the hypothetical scour protection by increasing the bed roughness for the area which had been assumed to be covered by stones as a scour protector. Their work led to a better understanding of the possible increase in bed shear stress due to presence of scour protectors and the identification of affected areas. Liu and García (2008) introduced a model for local sediment scour around piles under wave impact which included both bedload and

suspended load transport components. Their flow model employed the standard $k-\varepsilon$ turbulence closure model. They validated their model against experimental data from Sumer and Fredsøe (2001b). Khosronejad *et al.* (2012) carried out experimental and numerical investigation of scour around bridge piers with cylindrical, square, and diamond cross-section shapes. They used the fluid–structure interaction curvilinear immersed boundary (FSI-CURVIB) method by Khosronejad *et al.* (2011) to handle the moveable bed of the channel with embedded hydraulic structures. They applied the Unsteady Reynolds Averaged Navier-Stokes (URANS) in combination with the $k-\omega$ turbulence closure model to solve the flow field and found that the accuracy of their model could vary depending on the pier’s cross-section shape.

Escauriaza and Sotiropoulos (2011) applied detached-eddy simulation (DES) approach to solve the hydrodynamic model to be able to accurately resolve most of the turbulent stresses produced by the HSVs and used a bedload transport model which was inspired by works of Kovacs and Parker (1994) and Parker *et al.* (2003). They reported that their model was able to reproduce most of the characteristics observed by Dargahi (1990) during initial scour around the cylindrical pile. Kim *et al.* (2014), for the first time, employed Large Eddy Simulation (LES) approach to solve the Navier-Stokes equations and followed an approach similar to work of De Ruiter (1983) for sediment transport. They validated their model by experimental data from Khosronejad *et al.* (2012). Stahlmann and Schlurmann (2012) and Stahlmann (2013) highlighted the lack of knowledge and understanding of scour progression around complex offshore foundation structures, and introduced a model which was highly inspired by the work of Roulund *et al.* (2005). The model solves the combined waves and tidal current flow fields and its sediment transport model considers both bedload and suspended-load, and was applied to simulate scour around wind turbines with tripod foundations. As most recent works, the works of Sumer *et al.* (2014), Baykal *et al.* (2015) and Baykal *et al.* (2017) can be mentioned which used a similar hydro-morphodynamic model. However, their model followed the classical approach, it benefited from a truncated computational domain to solve an advection-diffusion equation for the suspended load model. Baykal *et al.* (2015) applied the model to investigate the effects of lee-wake vortices, as well as suspended sediment transport on scouring around a vertical pile on steady current. On the other hand, Sumer *et al.* (2014) and Baykal *et al.* (2017) used the model to investigate backfilling of a scour hole around circular piles. They validated their results against the experimental outputs from Sumer *et al.* (2012). In another work, Omara *et al.* (2019) applied FLOW-3D to numerically estimate the flow behavior and scour depth around vertical and inclined bridge piers. The URANS equations in combination with the RNG $k-\varepsilon$ turbulence model was used to solve flow field while their sediment transport models included both bedload and suspended load. The model was validated against the experimental data from Ghiassi and Abbasnia (2013) for scour depth around a square pier. They pointed out that the prediction capability of the model was attached to the pier shape and its inclined direction.

Many studies, including the ones mentioned above, have successfully applied the classical approach in the investigation of scouring around vertical circular cylinders. Nevertheless, a review of previous numerical works on local scour around piers with different cross-section shapes revealed that the accuracy of these hydro-morphodynamic models in determining local scour varies with the piers cross-section shapes (e.g., works of Khosronejad *et al.* (2012) and Omara *et al.* (2019)). This limitation challenges the capability of the hydrodynamic part of the classical models in predicting the strength of formed HSVs upstream of mounted piers with different cross-section shapes (Khosronejad *et al.* 2012). In the present work, URANS equations in combination with the $k-\omega$ SST turbulence closure model is adopted to solve the hydrodynamic part of the model. The $k-\omega$ SST turbulence model has a proven capability in predicting adverse pressure gradients and separation

flow (Menter 1992). As the physical modelling of local scour is a time-consuming process, the low computational cost and high accuracy of this combination in simulating the main turbulence structures around piles/piers are desirable. In addition, proper attention is given to adjust the height of the centre of the first layer of the computational cells closest to the bed from the bed to ensure the requirements of the hydrodynamic and morphodynamic part of the model are satisfied. These considerations lead to propose a reliable tool for prediction of scour around piers with different cross-section shapes.

In the next section, a description of the mathematical model, including details of the proposed hydro- and morphodynamic models are briefly described. In section 3, the capability of the model in terms of prediction of the temporal development of local scour and the deformed bed in equilibrium condition is examined around circular, square and diamond piers. These cases are chosen as the strength of the HSVs is different around them. Observations by Khosronejad *et al.* (2012) determined the formation of strong HSVs upstream of the circular and square piers, while very weak HSVs were found for the case of diamond piers. Finally, in the conclusion section, the main contribution of this work is presented.

2. Description of the mathematical model

For the purpose of the present study, a model is implemented in the OpenFOAM® framework using the classic modeling approach. In this manner, at each time step, first, the hydrodynamic model is solved on the 3D computational mesh. Second, the flow field results are used to calculate the bed shear stress, as the primary parameter for solving sediment transport models. Then, the bedload model on a 2D mesh, in accordance with the bed boundary, and the suspended load model on a 3D computational mesh are passively solved. Finally, the results of the sediment transport model are reflected by solving the mass conservation equation over the 2D mesh and transferring the results as a deformation on the bed. The deformed mesh is used as a renewed computational mesh for the next time step of the solution.

2.1 Hydrodynamic model

The model only solves the water-phase in the computational domain. Hence, the domain is limited by a water-air interface at the top. This is a valid assumption for almost all practical cases as long as the ratio of the inertial force to the gravitational force, Froude number (Fr), is small (e.g., $Fr < 0.2$) in the flow (Roulund *et al.* 2005). The URANS equations are employed to solve a single-phase incompressible flow which in the Cartesian coordinate system with the convention of Einstein's summation are as follows

$$\frac{\partial u_i}{\partial x_i} = 0 \quad (1)$$

$$\frac{\partial u_i}{\partial t} + u_j \frac{\partial u_i}{\partial x_j} = f_i - \frac{1}{\rho} \frac{\partial P}{\partial x_i} + \vartheta \frac{\partial^2 u_i}{\partial x_i \partial x_j} + \frac{1}{\rho} \frac{\partial \tau_{ij}}{\partial x_j} \quad (2)$$

where u_i and f_i are the ensemble average velocity and the body force in the x_i direction respectively, t is the time, ρ is the fluid density, P is the mean pressure, ϑ is the molecular kinematic viscosity of fluid and τ_{ij} is the Reynolds stress component which is modeled using the

$k-\omega$ SST turbulence closure model. The PISO algorithm by Issa (1986) is chosen for solving the hydrodynamic model with a Courant number of $Co < 0.5$ to satisfy the numerical stability of solution.

2.1.1 Boundary conditions

The boundaries of the computational domain for all simulations include top, sides, outlet, inlet, cylinder body surface, and bed, as shown in Fig. 1. The top boundary which simulates the water-air interface is adapted with a slip boundary condition. The slip boundary condition behaves differently for different types of variables. For the scalar quantities (e.g., pressure), it simply uses Neumann condition (wall-normal zero gradients) at the boundary. However, in the case of vectorial variables (e.g., velocity), the tangential component to the boundary surface of the quantities is treated with Neumann condition (wall-normal zero gradients), while the normal component is handled with Dirichlet boundary condition (zero value). The symmetry boundary condition is considered at the sides of the computational domain for all quantities, which considering the ratio of the pier width to flume width in the experimental setups is justifiable as its effects are negligible. The outlet is treated with zero values for the gradient of all quantities except for the pressure, which is equal to zero at the outlet boundary. The approaching flow condition at the inlet is achieved using different methods which are described separately for each simulation in the result and discussion section. In order to have an accurate estimation of flow velocity near the wall, which is essential for the calculation of shear velocity and bed shear stress, near-wall treatment is applied. The walls which included mobile bed boundary and pier's body are treated by Cebeci and Bradshaw (1977) near-wall treatment model which is originally suggested for the log-layer region of the boundary layer. Therefore, the center of the first layer of the cells next to the wall should be placed in the logarithmic region of the boundary layer. Based on Cebeci and Bradshaw (1977), where the roughness of the surface is known, the near-wall treatment for the logarithmic region of the boundary layer can be defined by

$$u^+ = \frac{1}{\kappa} \ln(Ey^+) - \Delta B \quad (3)$$

$$u^+ = \frac{u}{u_f}, \quad y^+ = \frac{u_f y}{\nu} \quad (4)$$

where u^+ and y^+ are non-dimensional velocity and distance for the log-low region in the equilibrium turbulent boundary layer, respectively, u_f is friction velocity, y is the distance of the center of the first layer of the mesh from the wall, and $E = 9.8$ is the roughness-dependent constant. Substituting u^+ and y^+ from Eq. (4) into Eq. (3), the only unknown variable in Eq. (3) is the friction velocity which is calculated following the Newton-Raphson method. ΔB depends on the wall roughness and is calculated using equations provided by Cebeci and Bradshaw (1977). This approach provides three regimes based on the value of the dimensionless (normalized) roughness height (k_s^+) defined by

$$k_s^+ = \frac{k_s u_f}{\nu} \quad (5)$$

ΔB in the three regimes is obtained as

$$\begin{array}{ll} \text{Hydrodynamically smooth} & \Delta B = 0 \\ \text{surface } (k_s^+ < 2.25): & \end{array} \quad (6)$$

Transitional surface ($2.25 \leq k_s^+ \leq 90$):

$$\Delta B = \frac{1}{\kappa} \ln \left[\frac{k_s^+ - 2.25}{87.75} + C_s k_s^+ \right] \sin[0.4258 (\ln k_s^+ - 0.811)] \quad (7)$$

Fully-rough surface ($k_s^+ > 90$):

$$\Delta B = \frac{1}{\kappa} \ln[1 + C_s k_s^+] \quad (8)$$

where k_s is the equivalent roughness height and C_s is the roughness constant. The value of turbulent properties (kinematic energy, k , and turbulence frequency, ω) needs to be determined near the walls. In the present setup, the turbulence kinematic energy, k , near the wall is satisfied by Neumann condition for both smooth and rough walls (Nezu 1977, Sumer *et al.* 2001, Sumer *et al.* 2003, Fuhrman *et al.* 2010). The turbulence frequency, ω , for the first layer of cells next to the wall is calculated following Ferziger *et al.* (2008) which is valid for the logarithmic region of the boundary layer

$$\omega = \frac{\sqrt{k}}{C_\mu^{0.25} \kappa y} \quad (9)$$

where C_μ has a value of 0.09.

2.2 Bed shear stress

The hydrodynamic and sediment transport models are connected through the bed shear stress since the calculated bed shear stress from the hydrodynamic model serves as the primary input parameter to the morphodynamic model. Therefore, an accurate calculation of bed shear stress is essential for obtaining realistic sediment transport results. Here, the vector of the bed shear stress acting on the wall is calculated from the inner product of the stress tensor, \mathbf{T} , and the unit normal vector of the face of the wall (\vec{n})

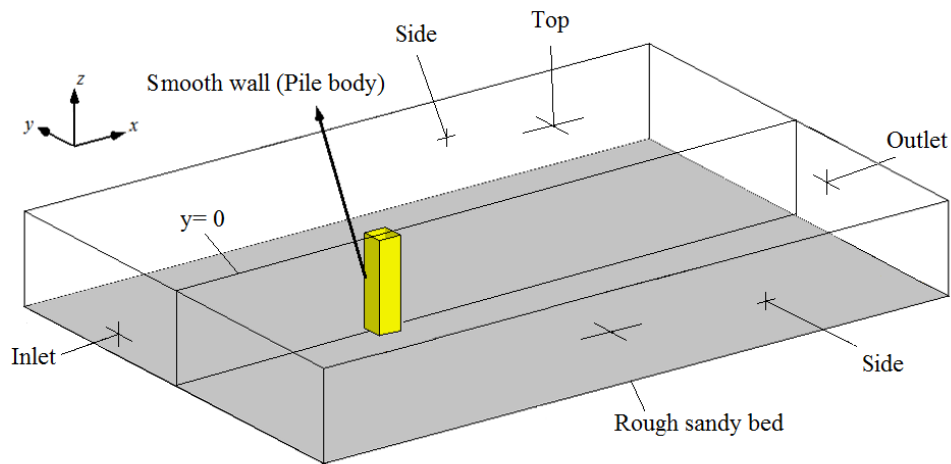


Fig. 1 Boundaries of the computational domain for test case of scouring around a square pier

$$\mathbf{T} = (v_t + \nu)(\nabla\mathbf{U} + \nabla\mathbf{U}^T) \quad (10)$$

$$\vec{\tau} = \mathbf{T} \cdot \vec{n} \quad (11)$$

where v_t is the turbulence viscosity defined by

$$v_t = \nu \left(\frac{y^+ \kappa}{\ln(Ey^+/e^{\kappa\Delta B})} - 1 \right) \quad (12)$$

where $\kappa = 0.4$ is the von Karman constant.

2.3 Sediment transport model

The adopted sediment transport model includes bedload and suspended load components. The bedload model computes the flux of the sediments that roll, slide or jump along the bed in a thin layer very close to the bed. For sediments transported above the bedload layer, the suspended load model calculates the sediment flux. These two sediment transport modes are separated by a hypothetical layer called the reference level. The bedload rate, q_B , is calculated based on the model given by Roulund *et al.* (2005), which is an extension of Engelund and Fredsøe (1976) model for a 2D bed. To solve the suspended load part of the model, the advection-diffusion equation is chosen to fulfill the case of non-uniform and transient flow around structures

$$\frac{\partial c}{\partial t} + \nabla \cdot [(\vec{u} + \vec{w}_s)c] = \nabla \cdot \left[\left(\vartheta + \frac{\vartheta_t}{\sigma_c} \right) \nabla c \right] + S_c \quad (13)$$

where c is the volumetric (dimensionless) suspended sediment concentration, \vec{u} and \vec{w}_s are the fluid velocity and sediment fall velocity vectors, respectively. $\vartheta + \vartheta_t/\sigma_c$ is the sediment diffusivity coefficient, where ϑ is the kinematic viscosity of the fluid, ϑ_t is the turbulence viscosity and σ_c is the concentration-dependent turbulent Schmidt number which is chosen as 0.8 similar to Liang and Cheng (2005). S_c is the source/sink term for the entrainment, E_Δ , and deposition rate, D_Δ , $S_c = E_\Delta - D_\Delta$. The entrainment rate, E_Δ , is obtained from

$$E_\Delta = c_e w_s \quad (14)$$

where w_s can be calculated by the method proposed by Soulsby (1997) and c_e is the equilibrium (reference) concentration of suspended load at a reference level height from the bed, Δ . c_e as described by Rijn (1984) given by

$$c_e = 0.015 \frac{d_{50} T^{1.5}}{\Delta d_*^{0.3}} \quad (15)$$

where Δ is adopted based on the average particle diameter, d_{50} , and in the range of $3d_{50}$ to $4d_{50}$. In Eq. (15), T is the dimensionless transport stage parameter

$$T = \frac{\theta - \theta_c}{\theta_c} \quad (16)$$

where θ is Shields parameter, and θ_c is the critical Shields parameter corresponding to the initiation of sand particle motion on a horizontal bed, and d_* is non-dimensional grain size

$$d_* = \left[\frac{g(s-1)}{g^2} \right]^{1/3} d_{50} \quad (17)$$

where, g is the acceleration of gravity, and s is relative density of the sand. The deposition rate, D_Δ , is obtained from the approach applied by Liu and García (2008)

$$D_{\Delta} = c_b w_s \quad (18)$$

where c_b is the sediment concentration at the reference level.

In the present study, the first layer of computational cells closest to the bed is adjusted to be located at the distance of $3d_{50}$ to $4d_{50}$ from the bed in accordance with the adopted reference level height from the bed. Hence, the sediment concentration at the first layer of mesh closest to the bed is equal to the sediment concentration at the reference level, c_b . This condition is initially checked for all applied test cases, however, due to the expansion and contraction of the meshes due to the bed deformation in simulation process, some minor deviations may occur.

In the present model, both hydrodynamic and morphodynamic models are solved in each simulation time step and calculated changes as a result of solving mass conservation equation by Exner (1925) are implemented as a bed deformation in the computational domain. A sand sliding method, similar to the one used in Roulund *et al.* (2005), is also employed to avoid unreal bed slopes. To smooth the internal domain base on the deformed bed in the vertical direction, the Laplacian operator smoothing approach is considered to control mesh motion.

3. Results and discussions

To ensure that the applied coupled model is capable of predicting the local scour progression around vertical piers with different cross-section shapes, it is validated against three experimental test results reported by Roulund *et al.* (2005) and Khosronejad *et al.* (2012). In the first test case, the experimental measurements from Roulund *et al.* (2005) in the temporal development of local scour around a circular pier under live-bed condition is provided. In the second and third test cases, the experimental data from Khosronejad *et al.* (2012) in the formation of scour holes around square and diamond piers under clear-water condition is presented.

3.1 Scouring around a circular pier

3.1.1 Experimental data

This experiment was conducted in a flume, 10 m long and 4 m wide. A 0.1 m diameter pile with the hydraulically smooth body was fixed at 6.6 m downstream of the inlet section. The bed was covered with sand with a particle diameter of $d_{50} = 0.26$ mm. The test was conducted under live-bed and steady current flow. The water depth in the experiment was maintained at 0.4 m and the depth average velocity was $U = 0.46$ m/s. Fig. 2 shows the details of the test flume.

3.1.2 Numerical simulation

An initial mesh dependency study was done and a 3D mesh with around 400,000 cells was chosen as the top view of it is shown in Fig. 3. In this test case, the height of the center of the first layer of mesh closest to the bed was considered 1 mm (around $4d_{50}$) to satisfy the morphodynamic requirement of the model. With a good estimation, these points (centers) are located in the logarithmic region of the hydrodynamic boundary layer. The bed boundary was considered as a mobile bed with a roughness factor of $k_s = 2.5 d_{50}$ and the critical Shields parameter for the horizontal bed of $\theta_{co} = 0.05$ as proposed by Roulund *et al.* (2005). The inlet boundary was supplied with the velocity profile obtained from the curve fitting of the provided profile in Roulund *et al.* (2005) as shown in Fig. 4.

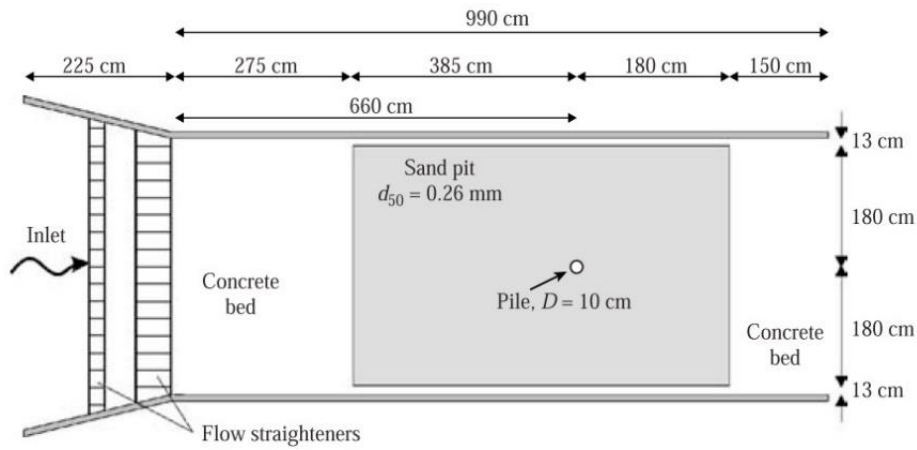


Fig. 2 Test conditions for scouring around a circular pier (Roulund *et al.* 2005)

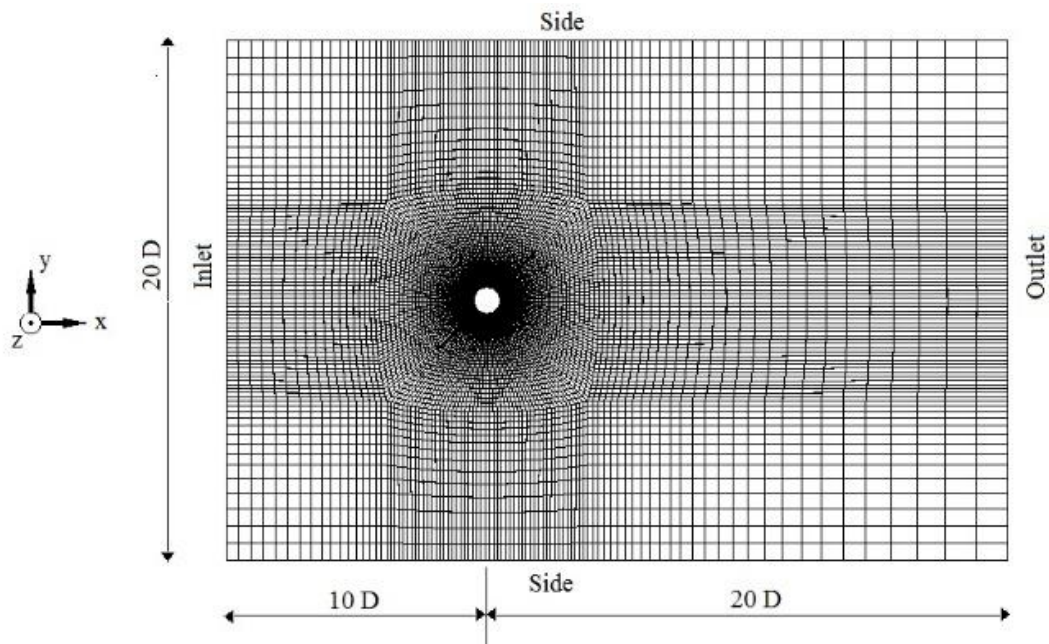


Fig. 3 Top view of generated mesh for test case of scouring around a circular pier

The experimental test reached equilibrium scour stage after around 2 hours. However, the changes in the results after the first hour were small. Hence, to reduce the required simulation time, the model was only run for $T = 1$ hour of physical time which required around 3 months of simulation time

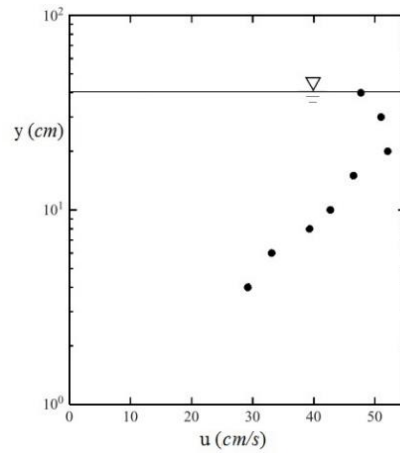


Fig. 4 Undisturbed mean flow velocity profile (Roulund *et al.* 2005)

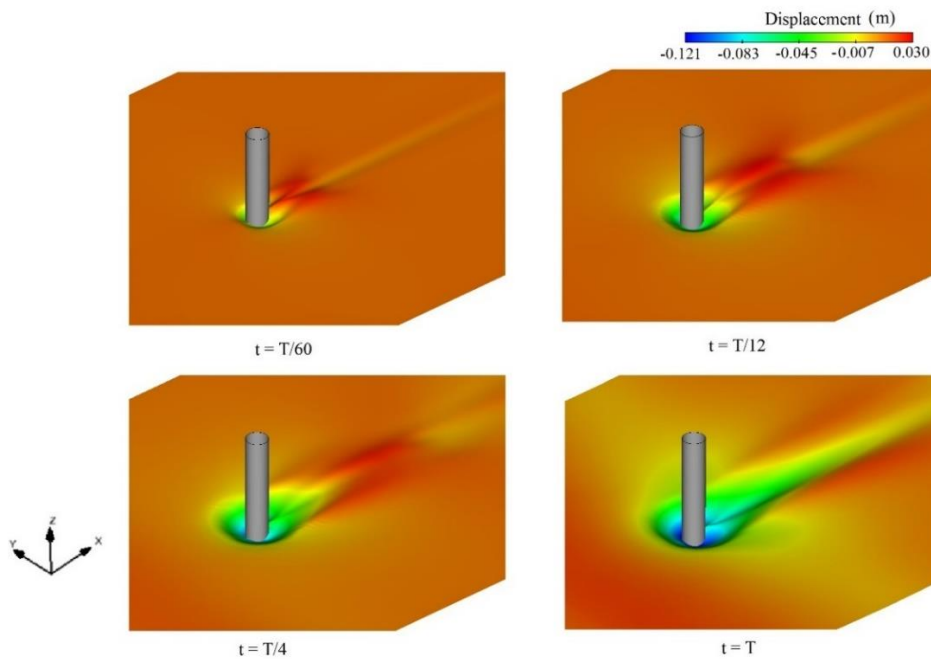


Fig. 5 Simulated bed displacement at 4 different times of the simulation $t = T/60, T/12, T/4, T$

on a 2.3 GHz CPU with 8 GB RAM. Fig. 5 shows a sequence of simulated bed deformation pictures at times $t = T/60, T/12, T/4, T$ from the start of the simulation. It is observed that the deformation of the bed and scouring adjacent to the pier starts from early stages of the simulation and extends in terms of the hole depth and the area affected by it. In Fig. 6, the evolution of the scour hole in terms

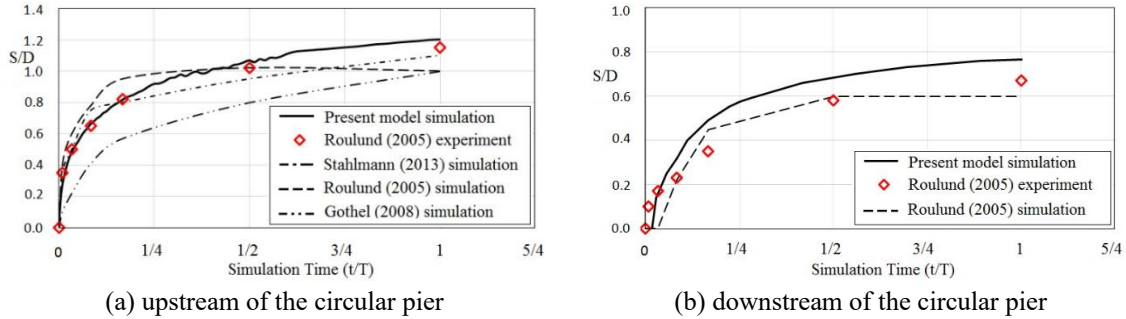


Fig 6. Changes in maximum scour depth with time

of the scour depth, S , in front and back of the pile, in the form of dimensionless scour depth, S/D , is compared with the experimental and simulation results of Roulund *et al.* (2005), Stahlmann (2013) and Gothel (2008). Dargahi (1990) pointed out that there is an initial stage before the beginning of scouring and formation of HSVs upstream of the piers. This initial stage is the corresponding time for the expansion of the boundary layer over the bed. It is here assumed that the measured scouring experimental data from Roulund *et al.* (2005) were based on the start of the formation of HSVs and the observation of sign of scouring upstream of the pile as it can be derived from Roulund's results. The results of the present work (Solid line in Fig. 6) has a very good agreement with the experimental results in terms of predicting the maximum scour hole during evolution. The maximum discrepancy in the prediction of maximum scour hole depth is less than 4.6% during the evolution process, however, the model overestimates the scour depth at the back of the pier from an early stage of the simulation and the maximum difference happens after 5 minutes of simulation which is around 30%.

3.2 Scouring around a diamond and square pier

3.2.1 Experimental data

The formation of HSV upstream of the mounted piers is one of the main factors in the development of the local scour. Khosronejad *et al.* (2012) mentioned that the intensity of the main HSV is in connection with the bluntness factor (BF). The bluntness factor is a character of describing the mounted pier nose geometry (Fleming *et al.* 1991, Fleming *et al.* 1993)

$$BF = \frac{1}{2} \frac{R}{X} \left(\frac{D_w}{S_D} + \frac{S_D}{X} \right) \quad (19)$$

where R is the radius of the leading-edge, X is the length of the chordwise position of the nose from the maximum width of the pier D_w , and S_D is the distance from the leading edge along the structure surface to the maximum width of the pier. Piers with larger bluntness factor face stronger HSVs. To evaluate the robustness of the developed model on the evolution of scour hole around piers with different cross-section shapes, the model was verified against experimental cases from Khosronejad *et al.* (2012) for square and diamond piers with $BF \rightarrow \infty$ and 0, respectively.

The tests were conducted in a flume with 10 m long and 1.21 m wide. In both tests, the piers were mounted at 4 m downstream of the flume inlet. Tests were conducted for a square-shaped cylinder with an edge length of 16.51 cm but with 90° and 45° orientation angles to the flow corresponding to the square and diamond piers. Hence in the case of the square pier, the pier width

to the flow direction, w_p , was 16.51 cm and for the diamond pier, 23.35 cm. The piers' body was considered as a hydraulically smooth surface. Both tests were carried out under clear-water conditions and the bed was covered with sand particles with the mean diameter of $d_{50} = 0.85$ mm, while different flow condition was applied for the tests. For the square pier test, the experiment was run for the undisturbed flow with a mean average velocity of $U = 0.22$ m/s and uniform flow depth of 13.9 cm, while the mean averaged velocity and flow depth of 0.21 m/s and 15.7 cm were considered for the case of the diamond pier test.

3.2.2 Numerical simulation

Numerical simulation for both cases was followed in computational domains 3 m long and 2 m wide where the piers were located 1 m downstream of the inlet. The height of the domain was set equal to the water depth in each case. In these test cases, the height of the center of the first layer of mesh closest to the bed was considered 2.5 mm to satisfy the hydrodynamic and morphodynamic requirements of the model. A mesh dependency test was also done for these cases and 3D meshes with around 350,000 cells were chosen. The approaching flow attributes at the inlet was supplied by a preliminary hydrodynamic simulation which was conducted for a domain with the same condition as the original mesh and with 3 m length but without the presence of the pier. The length of the preliminary simulation was kept 3 m to provide the approaching flow with the same condition as the experiments. The bed Nikuradse equivalent sand roughness for this case was considered equal to $3d_{50}$ as suggested by Khosronejad *et al.* (2012) and the critical Shields parameter value for horizontal bed was calculated from the equation proposed by Soulsby and Whitehouse (1997)

$$\theta_{c0} = \frac{0.3}{1+1.2d_*} + 0.055(1 - e^{-0.02d_*}) \quad (20)$$

Fig. 7 displays the temporal evolution of scour depth for both diamond and square piers. The results from present simulations are compared with simulation and experimental results from Khosronejad *et al.* (2012). In the case of the square pier, the result from the present model outperforms the numerical model of Khosronejad *et al.* (2012), while both simulation results underestimated the scour progression. The numerical results for diamond pier are roughly similar. The measurement of scour depth in equilibrium condition for the present simulations shows the differences of 6.7% and 13.1% from the experiment data for the square and diamond pier cases, respectively.

A comparison between the bed topography in equilibrium condition for the results of the present simulations and the laboratory measurements from Khosronejad *et al.* (2012) for the diamond and square piers is shown in Fig. 8. The experimental data is only presented for one side of the symmetry plane $y=0$ in Khosronejad *et al.* (2012). Hence, for the sake of comparison, in each case, the experimental results are provided on the bottom side and the present model numerical results on the top side. In the square pier case, Khosronejad *et al.* (2012) as a result of laboratory measurements pointed out that the maximum scour depth occurred in the front corners of the pier, while the area with significant depth was seen around the nose of the pier. The present numerical model also found the maximum scour depth in the front corners of the pier, however, it failed to accurately predict the depth of the scoured area around the front side of the pier. In contrast, the maximum deposition height position given by the numerical model is in accordance with experimental measurements. For the diamond pier, a good agreement in the position of the maximum scour depth and deposition height is observed between the numerical simulation results and experimental data. The obtained

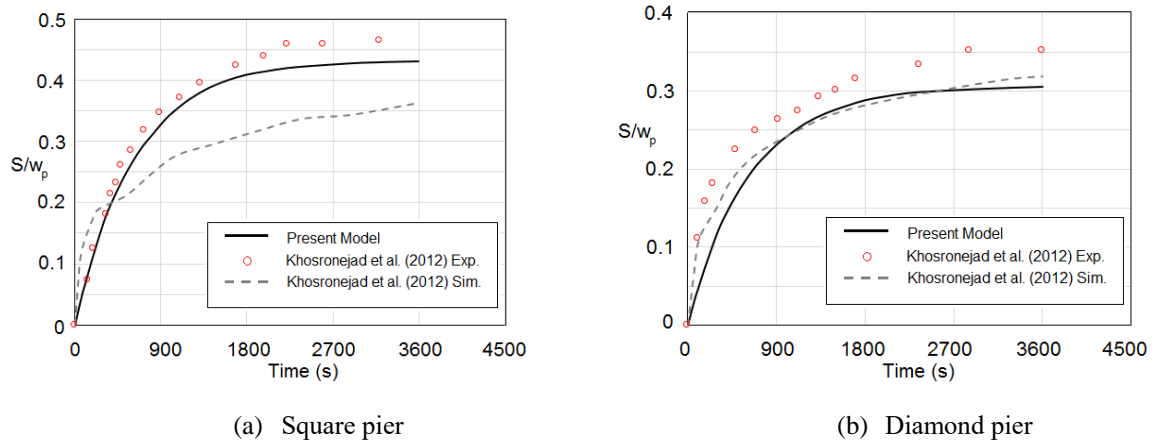


Fig. 7 Changes in scour depth with time in case of (a) square and (b) diamond pier

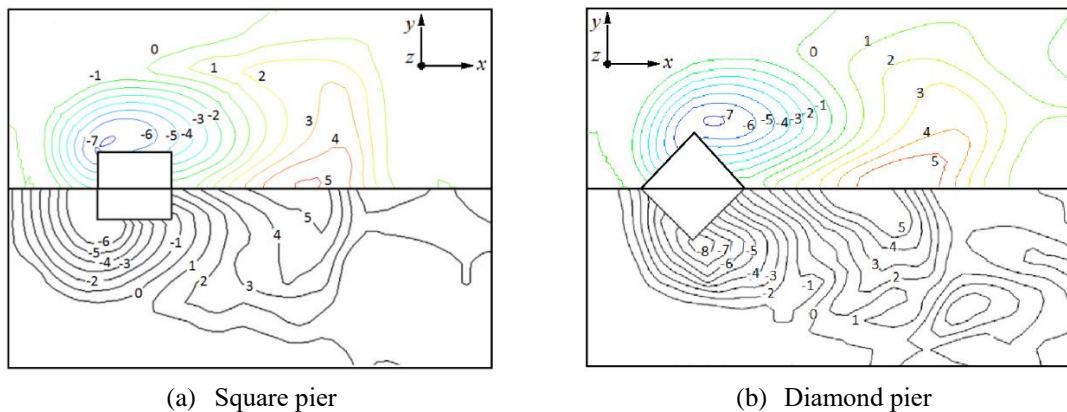


Fig. 8 Comparison of the present model simulation (top) and measured (bottom) bed topography at equilibrium condition (The measurement unit is cm)

results from the simulations indicated that the present model has a good capability in predicting the main characteristics of scour around the square and diamond piers.

4. Conclusions

In the present study, a 3D numerical model for the prediction of scour evolution around vertical cylinders was developed and implemented in OpenFOAM® framework. A coupled approach was applied for combining the hydrodynamic and morphodynamic parts. The proposed model is validated against the empirical measurements of local scour development around single vertical piers with circular, square, and diamond cross-section shapes obtained from the literature. The measurement of scour depth in equilibrium condition for the simulations revealed the differences of

4.6%, 6.7% and 13.1% from the experimental measurements for the circular, square, and diamond pier cases, respectively. The model displayed a remarkable performance in the prediction of scour around circular and square piers where HSVs have a leading impact on scour progression. On the other hand, the maximum deviation was found in the case of the diamond pier where HSVs are weak and have minimum impact on the formation of local scour. Overall, the results confirm that the prediction capability of the present model is almost independent of the strength of the formed HSVs and pier cross-section shapes.

References

- Agui, J.H. and Andreopoulos, J. (1992), "Experimental investigation of a three-dimensional boundary layer flow in the vicinity of an upright wall mounted cylinder (data bank contribution)".
- Baker, C.J. (1980), "The turbulent horseshoe vortex", *J. Wind Eng. Ind. Aerod.*, **6**, 9-23.
- Baykal, C., Sumer, B.M., Fuhrman, D.R., Jacobsen, N.G. and Fredsøe, J. (2015), "Numerical investigation of flow and scour around a vertical circular cylinder", *Philosoph. T. Roy. Soc. A: Math. Phys. Eng. Sci.*, **373**, <https://doi.org/10.1098/rsta.2014.0104>.
- Baykal, C., Sumer, B.M., Fuhrman, D.R., Jacobsen, N.G. and Fredsøe, J. (2017), "Numerical simulation of scour and backfilling processes around a circular pile in waves", *Coast. Eng.*, **122**, 87-107.
- Cebeci, T. and Bradshaw, P. (1977), "Momentum transfer in boundary layers", *Washington, DC, Hemisphere Publishing Corp.; New York, McGraw-Hill Book Co.*
- Dargahi, B. (1989), "The turbulent flow field around a circular cylinder", *Exp. Fluid.*, **8**, 1-12.
- Dargahi, B. (1990), "Controlling mechanism of local scouring", *J. Hydraul. Eng. -ASCE*, **116**, 1197-1214.
- De Ruiter, J.C.C. (1983), "Incipient motion and pick-up of sediment as function of local variables", *unpublished notes, Delft Hydraulics, Delft.*
- Dey, S., Bose, S.K. and Sastry, G.L.N. (1995), "Clear water scour at circular piers: a model", *J. Hydraul. Eng. -ASCE*, **121**, 869-876.
- Engelund, F. and Fredsøe, J. (1976), "A sediment transport model for straight alluvial channels", *Hydrology Res.*, **7**, 293-306.
- Escauriaza, C. and Sotiropoulos, F. (2011), "Initial stages of erosion and bed form development in a turbulent flow around a cylindrical pier", *J. Geophys. Res.: Earth Surface*, **116**.
- Exner, F.M. (1925), "Über die wechselwirkung zwischen wasser und geschiebe in flussen", *Akad. Wiss. Wien Math. Naturwiss. Klasse*, **134**, 165-204.
- Ferziger, J.H., Perić, M. and Street, R.L. (2008), *Numerische Strömungsmechanik*, Springer.
- Fleming, J.L., Simpson, R.L., Cowling, J.E. and Devenport, W.J. (1993), "An experimental study of a turbulent wing-body junction and wake flow", *Exp. Fluid.*, **14**, 366-378.
- Fleming, J.L., Simpson, R.L. and Devenport, W. J. (1991), "An experimental study of a turbulent wing-body junction and wake flow (Technical Report, 1 Jun. 1989- 31 Aug. 1991)".
- Fuhrman, D.R., Duxen, M. and Jacobsen, N.G. (2010), "Physically-consistent wall boundary conditions for the $k-\omega$ turbulence model", *J. Hydraulic Res.*, **48**, 793-800.
- Ghiassi, R. and Abbasnia, A.H. (2013), "Investigation of vorticity effects on local scouring", *Arabian J. Sci. Eng.*, 537-548.
- Göthel, O. (2008), Numerical modeling of flow and wave-induced scour around vertical structures.
- Göthel, O. and Zielke, W. (2007), "Numerical Modelling of Scour at Offshore Wind Turbines", *Coast. Eng.*, **5**, 2343-2353.
- Graf, W.H. and Istiarto, I. (2002), "Flow pattern in the scour hole around a cylinder", *J. Hydraulic Res.*, **40**, 13-20.
- Hansen, E.A., Simonsen, H.J., Nielsen, A.W., Pedersen, J. and Høgedal, M. (2007), "Scour protection around offshore wind turbine foundations, full-scale measurements", 132-138.

- Issa, R.I. (1986), "Solution of the implicitly discretised fluid flow equations by operator-splitting", *J. Comput. Phys.*, **62**, 40-65.
- Khosronejad, A., Kang, S., Borazjani, I. and Sotiropoulos, F. (2011), "Curvilinear immersed boundary method for simulating coupled flow and bed morphodynamic interactions due to sediment transport phenomena", *Adv. Water Resour.*, **34**, 829-843.
- Khosronejad, A., Kang, S. and Sotiropoulos, F. (2012), "Experimental and computational investigation of local scour around bridge piers", *Adv. Water Resour.*, **37**, 73-85.
- Kim, H.S., Nabi, M., Kimura, I. and Shimizu, Y. (2014), "Numerical investigation of local scour at two adjacent cylinders", *Adv. Water Resour.*, **70**, 131-147.
- Kirkil, G., Constantinescu, G. and Ettema, R. (2005), The horseshoe vortex system around a circular bridge pier on equilibrium scoured bed, *Impacts of Global Climate Change*.
- Kirkil, G., Constantinescu, G. and Ettema, R. (2009), "Detached eddy simulation investigation of turbulence at a circular pier with scour hole", *J. Hydraul. Eng. -ASCE*, **135**, 888-901.
- Kirkil, G., Constantinescu, G. and Ettema, R. (2008), "Coherent structures in the flow field around a circular cylinder with scour hole", *J. Hydraul. Eng. -ASCE*, **134**, 572-587.
- Kovaacs, A. and Parker, G. (1994), "A new vectorial bedload formulation and its application to the time evolution of straight river channels", *J. Fluid Mech.*, **267**, 153-183.
- Liang, D. and Cheng, L. (2005), "Numerical model for wave-induced scour below a submarine pipeline", *J. Waterw Port Coast. Ocean Eng.*, **131**, 193-202.
- Liu, X. and García, M.H. (2008), "Three-dimensional numerical model with free water surface and mesh deformation for local sediment scour", *J. waterway, port, coast. ocean Eng.*, **134**, 203-217.
- Melville, B.W. and Chiew, Y.M. (1999), "Time scale for local scour at bridge piers", *J. Hydraul. Eng. -ASCE*, **125**, 59-65.
- Menter, F.R. (1992), "Improved two-equation $k-\omega$ turbulence models for aerodynamic flows. NASA STI". Recon Technical Report 93, 22809.
- Nezu, I. (1977), "Turbulent structure in open-channel flows", *English translation of the Japanese dissertation of Iehisa Nezu*.
- Olsen, N.R.B. and Kjellesvig, H.M. (1998), "Three-dimensional numerical flow modeling for estimation of maximum local scour depth", *J. Hydraul. Res.*, **36**, 579-590.
- Olsen, N.R.B. and Melaaen, M.C. (1993), "Three-dimensional calculation of scour around cylinders", *J. Hydraul. Eng. -ASCE*, **119**, 1048-1054.
- Omara, H., Elsayed, S.M., Abdeelaal, G.M., Abd-Elhamid, H.F. and Tawfik, A. (2019), "Hydromorphological numerical model of the local scour process around bridge piers", *Arabian J. Sci. Eng.*, **44**, 4183-4199.
- Parker, G., Seminara, G. and Solari, L. (2003), "Bed load at low Shields stress on arbitrarily sloping beds: Alternative entrainment formulation", *Water Resour. Res.*, **39**.
- Rijn, L.C.V. (1984), "Sediment transport, part II: suspended load transport", *J. Hydraul. Eng. -ASCE*, **110**, 1613-1641.
- Roulund, A., Sumer, B.M., Fredsøe, J. and Michelsen, J. (2005), "Numerical and experimental investigation of flow and scour around a circular pile", *J. Fluid Mech.*, **534**, 351-401.
- Salaheldin, T. M., Imran, J. and Chaudhry, M.H. (2004), "Numerical modeling of three-dimensional flow field around circular piers", *J. Hydraul. Eng. -ASCE*, **130**, 91-100.
- Seal, C.V. and Smith, C.R. (1999), "Visualization of a mechanism for three-dimensional interaction and near-wall eruption", *J. Fluid Mech.*, **394**, 193-203.
- Soulsby, R. (1997), *Dynamics of marine sands: a manual for practical applications*, Thomas Telford.
- Soulsby, R. and Whitehouse, R. (1997), "Threshold of sediment motion in coastal environments", *Pacific Coasts and Ports'97: Proceedings of the 13th Australasian Coastal and Ocean Engineering Conference and the 6th Australasian Port and Harbour Conference*; Volume 1: Centre for Advanced Engineering, University of Canterbury, 145.
- Stahlmann, A. (2013), "Numerical and experimental modeling of scour at foundation structures for offshore wind turbines", *Int. Soc. Offshore Polar Engineers*.

- Stahlmann, A. and Schlurmann, T. (2012), "Numerical and Experimental Modeling of Scour at Tripod Foundations for Offshore Wind Turbines", *Proceedings of the 6th International Conference on Scour and Erosion*, Paris, France.
- Sumer, B. M., Baykal, C., Fuhrman, D.R., Jacobsen, N.G. and Fredsøe, J. (2014), "Numerical calculation of backfilling of scour holes".
- Sumer, B.M., Christiansen, N. and Fredsøe, J. (1993), "Influence of cross section on wave scour around piles", *J. waterway, port, coast. ocean engineering*, **119**, 477-495.
- Sumer, B.M., Chua, L.H.C., Cheng, N.S. and Fredsøe, J. (2003), "Influence of turbulence on bed load sediment transport", *J. Hydraul. Eng. -ASCE*, **129**, 585-596.
- Sumer, B.M., Cokgor, S. and Fredsøe, J. (2001), "Suction removal of sediment from between armor blocks", *J. Hydraul. Eng. -ASCE*, **127**, 293-306.
- Sumer, B.M. and Fredsøe, J. (2001a), "Scour around pile in combined waves and current", *J. Hydraul. Eng. - ASCE*, **127**, 403-411.
- Sumer, B.M. and Fredsøe, J. (2001b), "Wave scour around a large vertical circular cylinder", *J. Waterw Port Coast. Ocean Eng.*, **127**, 125-134.
- Sumer, B.M., Fredsøe, J. and Christiansen, N. (1992), "Scour around vertical pile in waves", *J. Waterw Port Coast. Ocean Eng.*, **118**, 15-31.
- Sumer, B.M., Petersen, T.U., Locatelli, L., Fredsøe, J., Musumeci, R.E. and Foti, E. (2012), "Backfilling of a scour hole around a pile in waves and current", *J. Waterw Port Coast. Ocean Eng.*, **139**, 9-23.
- Topczewski, Ł., Cieśla, J., Mikołajewski, P., Adamski, P. and Markowski, Z. (2016), "Monitoring of scour around bridge piers and abutments", *T. Res.Procedia*, **14**, 3963-3971.
- Tseng, M.H., Yen, C.L. and Song, C.C.S. (2000), "Computation of three-dimensional flow around square and circular piers", *Int.l J. Numer. Method, Fluid.*, **34**, 207-227.